ISSN 2176-5480

# Numerical Tests for an Improved Damage Evolution Law Based on CDM and with Two Calibration Points

**Carlos Filipe de Queiroz Araújo**
University of Brasilia, Faculty UnB at Gama, Área Especial de Indústria Projeção A – Gama, Setor Leste, Brasília/DF, 72444-240
carlinhosqa@gmail.com

**Lucival Malcher**
University of Brasilia, Faculty of Tecnology, Department of Mechanical Engineering, Brasília/DF
malcher@unb.br

**Guilherme Pacheco**
University of Brasilia, Faculty UnB at Gama, Área Especial de Indústria Projeção A – Gama, Setor Leste, Brasília/DF, 72444-240
guilhermepacheco09@gmail.com

**André Nepomuceno Trajano**
University of Brasilia, Faculty UnB at Gama, Área Especial de Indústria Projeção A – Gama, Setor Leste, Brasília/DF, 72444-240
andrentrajano@gmail.com

***Abstract.*** *In this contribution, it is proposed a numerical comparative study for an improved damage model, based on Continuum Damage Mechanics (CDM), dependent on third invariant and with two calibration points for determination of all materials parameters. In the first part, theoretical aspects of the constitutive model are presented as well as the implicit numerical integration algorithm, which is based on the operator split methodology and implemented in an academic finite element development. In the second part, numerical tests are carried out regarding the improved damage model and classical Lemaitre damage model. Furthermore, smooth bar, notched bars and shear specimens are used to evaluate the robustness of the improved constitutive model. Aspects, as the evolution of the damage parameter, evolution of the equivalent plastic strain, the reaction curve, the level of displacement at fracture and ability to predict the correct fracture onset are discussed.*

***Keywords:*** *damage model; third invariant; two calibration points*

## 1. INTRODUCTION

According to the thermodynamic of internal variable, the behavior of materials can be modeled by constitutive equations, taking into account its progressive degradation. These models are based on the assumption that the internal damage begins from micro-cracks and can be effectively represented by one or more associated internal variables that can represented by a scalar, a vector or a tensor. These variables, called damage variables are defined as a measure of defects within a representative volume (RVE). Its development should be defined through the constitutive thermodynamic relations, usually represented by a system of differential equations in time. Based on Continuum Damage Mechecanics (CDM), several constitutive models have been proposed, such as Lemaitre (1985), for damage caused by plastic flow, Chaboche (1984) and Murakami & Ohmo (1981), for creep damage, Krajeinovic & Fonseka (1981), for brittle damage, among others.

Despite of continuum advances, many questions remain open, such as modeling problems related to failure in metal, resulting from progressive deterioration associated with micro structural deformations. In such cases, the development of new and more refined constitutive models deserves careful consideration and, thus, the issue continues to be an excellent area of research and development. There are several technological processes that would benefit considerably from a better understanding and quantification of the different physical phenomena that occur near the rupture of ductile materials. The metal cutting, for example, is a technological process used in manufacturing a wide range of products and is currently employed by a large number of companies. The importance of this process is underlined by the fact that almost every object we

use in our society has one or more machined surfaces. Due to its high use, the effectiveness of this process has an impact on the quality and cost of the products obtained.

Based on the context presented, in this contribution a damage evolution law is proposed aims at detailed study and improvement of the damage model of Lemaitre (1985), with isotropic hardening and damage. The work begins with the study of the original model of Lemaitre through conventional specimens that result in different levels of triaxiality. Based on the results of this study, we aimed to demonstrate the vagueness of this formulation, with respect to the prediction of the correct time (displacement) and local potential for initiation of ductile fracture, when the loading condition imposed is presented away from the fixed point as calibration parameters of elasto-plastic and evolution of damage variable, such as hardening curve, the exponent and denominator of damage. After this preliminary analysis, the objective is to adjust the model of Lemaitre, regarding its accuracy and strong dependence of the calibration point. For this, it is proposed to create a function called "function denominator of damage", instead of the denominator of damage, which was originally presented as a material constant.

Regarding this modification, it is also proposed to define a new state potential and dissipation potential for the new model, thus maintaining the thermodynamic consistency of the formulation. A new evolution law for the damage variable is then deducted as well as other internal variables, such as plastic deformation and variable associated with isotropic hardening. A new numerical integration algorithm is suggested for the proposed formulation, based on the "split operator" methodology (Simo *et. al.*, 1998), and new numerical simulations are made in order to demonstrate the predictive ability of the new formulation, when it comes to determining the correct displacement at fracture, as well as the potential site for crack initiation.

## 2. CONSTITUTIVE FORMULATION

### 2.1. Stress triaxiality and third invariant effects.

Several factors have been systematically analysed in the study of ductile fracture, nevertheless, there are three factors that have gained increased interest: the hydrostatic stress ($p$), stress triaxiality ($\eta$), and the Lode angle ($\theta$) expressed by *Equations* (1-3) respectively (Brunig *et al*., 2008; Bai & Wierzbicki, 2008; Zadpoor *et al*., 2009; Tvergaard, 2008; Nahshon *et al*., 2008).

$$p = \frac{1}{3}\, tr\,(\boldsymbol{\sigma})\,, \tag{1}$$

$$\eta = -\frac{p}{q}\,, \tag{2}$$

$$\theta = \tan^{-1}\left\{\frac{1}{\sqrt{3}}\left[2\left(\frac{S_2 - S_3}{S_1 - S_3}\right) - 1\right]\right\}\,, \tag{3}$$

where $q = \sqrt{3/2\,\boldsymbol{S}:\boldsymbol{S}}$ is the von Mises equivalent stress, $\boldsymbol{S} = \boldsymbol{\sigma} - p\boldsymbol{I}$ is the deviatoric stress tensor and $S_1$, $S_2$ and $S_3$ are the components of the deviatoric stress tensor in the principal plane. The Lode angle can also be written as a function of the so-called normalized third invariant of the deviatoric stress tensor, as presented below

$$\theta = \frac{1}{3} arccos(\xi)\,, \tag{4}$$

where $\xi$ represents the normalized third invariant, that can be mathematically determined by a ratio between the third invariant and the von Mises equivalent stress

$$\xi = \left(\frac{r}{q}\right)^3\,. \tag{5}$$

The term $r$ represents the third invariant, alternatively, defined by Bai *et al*. (2007) and can be determined as following

$$r = \left[\frac{27}{2} J_3\right]^{1/3} = \left[\frac{27}{2} det(\boldsymbol{S})\right]^{1/3}, \quad (6)$$

where $J_3$ is the third invariant of the deviatoric stress tensor, $\boldsymbol{S}$. The Lode angle can also be normalized ($\bar{\theta}$) and this parameter is known as the normalized Lode angle (Bai & Wierzbicki, 2008).

$$\overline{\theta} = 1 - \frac{6\theta}{\pi}. \quad (7)$$

The range of $\bar{\theta}$ is $-1 \leq \bar{\theta} \leq 1$. According to many authors, the contribution of the effect of the third invariant is more severe than the contribution of the stress triaxiality effect in the plastic flow rule (see Bai *et al*, 2008 and Gao, 2011).

## 2.2. Damage evolution law

In this section, it will be proposed a new formulation for the Lemaitre damage evolution law, based on the creation of a function call "denominator of damage function", which is dependent on the level of stress triaxiality and the normalized third invariant. This function, based on phenomenological observations, replace the denominator of damage, in the original Lemaitre damage evolution law, which in turn is a constant, calibrated based on experimental results in a smooth specimen subjected to pure tensile. With the creation of the denominator of damage function, it is intended to increase the accuracy of Lemaitre's damage model, as regards the ability to predict the correct level of displacement at fracture for ductile materials. How was discussed previously, the Lemaitre model loses its accuracy with regard the predictive ability, when the applied loading condition, is presented away from the chosen point as the calibration condition of material parameters. This damage model can then behave premature, anticipating the start of a crack prior to the experimentally observed when the applied loading condition has a stress triaxiality level lower than the calibration point chosen. However, when the loading condition studied shows a level of stress triaxiality higher than the calibration point, the damage model can then predict the fracture onset so late compared to experimental observations in the literature. Figure 1 shows the behavior of the Lemaitre's damage model, according to the level of stress triaxiality of the load history applied in comparing to the calibration point.

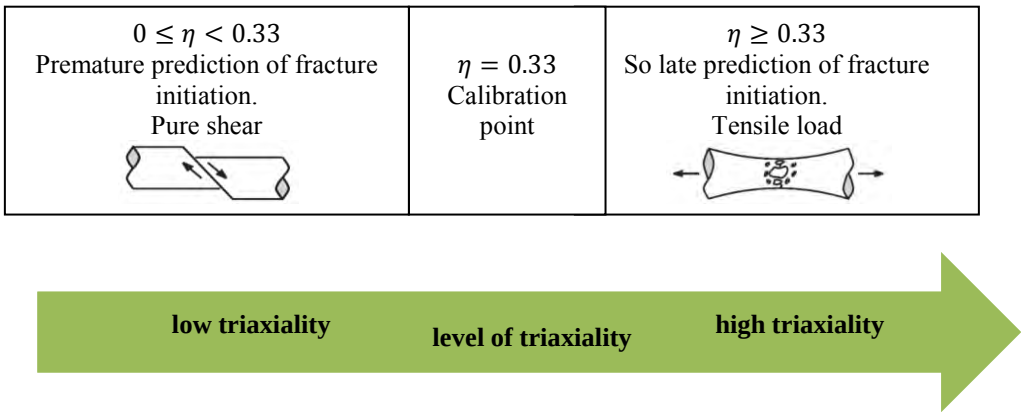


Figure 1. Behavior of Lemaitre´s model regarding the dependence of the calibration point.

### 2.2.1. High stress triaxiality region: ($\eta \geq 0.33$)

Regarding the region of high stress triaxiality, it is suggested to use a function dependent on the material parameters calibrated traditionally, i.e., by experimental results based on a pure tensile test on a smooth cylindrical specimen. Thus, the following expression is then phenomenological suggested as:

$$S'(\eta) = \frac{a}{3|\eta|}, \tag{8}$$

where $S'(\eta)$ represents the denominator of damage function for the region of high stress triaxiality, $\eta$ is the stress triaxiality and the term $a$ represents the material parameters to be calibrated or represents the denominator of damage calibrated by a cylindrical smooth bar specimen ($\eta = 0.33$). Equation 8 can be rewritten as:

$$S'(\eta) = \frac{S_{0.33}}{3|\eta|}, \tag{9}$$

where $S_{0.33}$ represents the denominator of damage calibrated by a cylindrical smooth bar specimen subjected to a pure tensile loading condition.

**2.2.2. Low stress triaxiality region:** ($0 \leq \eta < 0.33$)

For the region of low stress triaxiality, it is suggested to use the pure shear loading condition, $\eta = 0.0$, as the second calibration point. Thus, the following phenomenological equation can be defined:

$$S''(\xi) = b(1 - \xi^2), \tag{10}$$

where $S''(\xi)$ represents the denominator of damage function for low stress triaxiality region, the parameter $\xi$ is the normalized third invariant of the deviatoric stress tensor and the term $b$ represents a material parameter to be calibrated, i.e., it is the value of the denominator of damage calibrated by pure shear condition. The normalized third invariant is determined by the following expression:

$$\xi = \frac{(27/2)\det \boldsymbol{S}}{q^3}, \tag{11}$$

where $\boldsymbol{S}$ represents the deviatoric stress tensor and $q$ is the von Mises equivalent stress, which is determined by $q = \sqrt{(3/2)\boldsymbol{S}:\boldsymbol{S}}$. Equation 10 can be better represented by:

$$S\ (\xi) = S_{0.0}(1 - \xi^2), \tag{12}$$

where $S_{0.0}$ represents the denominator of damage calibrated by a pure shear loading condition.

For that the denominator of damage function can now be applied to wide range of stress triaxiality, Equations 9 and 12 need to be coupled, keeping the behavior already observed. The denominator function will then be dependent on both stress triaxiality and the normalized third invariant. The following expression represents the coupling behavior of the denominator of damage, within the regions of low and high stress triaxiality.

$$S(\eta, \xi) = \frac{S_{0.33}}{3|\eta| + \frac{S_{0.33}}{S_{0.0}}(1 - \xi^2)}. \tag{13}$$

where $S(\eta, \xi)$ represents the denominator of damage function for wide range of stress triaxiality. The denominator of damage function now requires two calibration points for the correct definition. It is necessary to determine the optimal value of $S$ for a pure shear loading ($S_{0.0}$) and for a pure tensile load, regarding a cylindrical smooth bar specimen ($S_{0.33}$). This function will take values as follows: under pure shear condition, the set of parameters $(\eta, \xi)$ are both equal to zero. Thus, replacing these values in Equation 12, it is also obtained exactly $S_{0.0}$. On the other hand, under high stress triaxiality condition, the denominator of damage will assume values less than or equal to $S_{0.33}$.

Table 1 presents a comparison between the values for the denominator obtained by the calibration procedure, regarding each loading condition and by Equation 13, for an aluminum alloy 2024-T351. In this comparison, it is observed a good agreement between both values.

Table 1. Assessment between values of *S* determined by calibration procedure and by the function suggested.

| Specimen | $\eta$ | $\xi$ | *S* (calibrated) | *S* (by Equation 13) |
|---|---|---|---|---|
| Butterfly | 0.00 | 0.0 | 8.3 | 8,3 |
| Smooth bar | 0.33 | 1.0 | 6.0 | 6.0 |
| Notched bar, *R=12 mm* | 0.47 | 1.0 | 4.1 | 4.2 |
| Notched bar, *R=4 mm* | 0.74 | 1.0 | 2.8 | 2.7 |

### 2.2.3. Coupling denominator of damage function and damage evolution law

The damage evolution law for Lemaitre's original model is described by Equation. Nevertheless, introducing the denominator of damage function $S(\eta,\xi)$, how was proposed above (Equation 13), replacing the denominator of damage $S$, we have:

$$\dot{D} = \frac{\dot{\gamma}}{1-D}\left[\frac{-Y}{S(\eta,\xi)}\right]^{s}, \tag{14}$$

where $S(\eta,\xi)$ represents the denominator of damage function. The material parameters $s$ is the so called exponent of damage, which is in general is equal to unity for most ductile materials.

Regarding the above modification applied to the Lemaitre's original damage model and assuming again the approach of the existence of a single dissipation potential given by the additive decomposition of the damage $\Psi^{d}$ and hardening $\Psi^{p}$ potentials, the new contribution due to the damage potential will be written as:

$$\Psi^{d} = \frac{S(\eta,\xi)}{(1-D)(s+1)}\left(\frac{-Y}{S(\eta,\xi)}\right)^{s+1}. \tag{15}$$

This expression is obtained assuming the integration procedure of Equation 14 in relation to the thermodynamic force associated to the damage, $Y$. Substituting Equation 15 in the additive decomposition of the dissipation potential, we have now:

$$\Psi = \Psi^{p} + \Psi^{d} = \Phi + \frac{S(\eta,\xi)}{(1-D)(s+1)}\left(\frac{-Y}{S(\eta,\xi)}\right)^{s+1}, \tag{16}$$

with defined by:

$$\Phi(\boldsymbol{\sigma}, R, D) = \frac{\sqrt{3J_2(\boldsymbol{S})}}{(1-D)} - (\sigma_0 + R(r)). \tag{17}$$

It can be highlight that the kinematic hardening was neglected.

### 2.2.4. Definition of the plastic flow rule: associative model

Regarding an associative plasticity, the so called yield function is then adopted as a flow potential or dissipation potential, $\Psi \equiv \Phi$ . In this case, the associative implies that the plastic strain rate is a tensor normal to the yield surface, regarding the deviatoric plane. Thus, the evolution equation for the plastic strain $\boldsymbol{\varepsilon}^{p}$, isotropic hardening internal variable $r$ and damage $D$, are obtained according as follow:

$$\dot{\boldsymbol{\varepsilon}}^p = \dot{\gamma}\frac{\partial \Phi}{\partial \boldsymbol{\sigma}} = \dot{\gamma}\sqrt{\frac{3}{2}}\frac{\boldsymbol{S}}{(1-D)\|\boldsymbol{S}\|}$$
$$\dot{r} = -\dot{\gamma}\frac{\partial \Phi}{\partial R} = \dot{\gamma} \tag{18}$$
$$\dot{D} = \dot{\gamma}\frac{\partial \Psi^p}{\partial Y} = \frac{\dot{\gamma}}{1-D}\left(\frac{-Y}{S(\eta,\xi)}\right)^s$$

Thus, the improved Lemaitre's model, regarding the associative plasticity, isotropic hardening, isotropic damage and the denominator of damage function, can be briefly written according Box 1.

Box 1. Improved Lemaitre's model with the denominator of damage function, isotropic hardening and damage.

*(i)* Additive decomposition of strain:

$$\boldsymbol{\varepsilon} = \boldsymbol{\varepsilon}^e + \boldsymbol{\varepsilon}^p$$

*(ii)* Elastic law with damage coupled:

$$\boldsymbol{\sigma} = (1-D)\mathbb{D}:\boldsymbol{\varepsilon}^e$$

*(iii)* Yield function:

$$(\boldsymbol{\sigma}, R, D) = \frac{\sqrt{3J_2(\boldsymbol{S})}}{(1-D)} - (\sigma_0 + R(r))$$

*(iv)* Plastic flow rule and evolution equation for $r$ and $D$:

$$\dot{\boldsymbol{\varepsilon}}^p = \dot{\gamma}\sqrt{\frac{3}{2}}\frac{\boldsymbol{S}}{(1-D)\|\boldsymbol{S}\|}$$
$$\dot{r} = \dot{\gamma}$$
$$\dot{D} = \frac{\dot{\gamma}}{1-D}\left(\frac{-Y}{S(\eta,\xi)}\right)^s$$

with:

$$-Y = \frac{1}{2E(1-D)^2}\left[\frac{2}{3}(1-\upsilon)q^2 + 3(1-2\upsilon)p^2\right]$$
$$S(\eta,\xi) = \frac{S_{0.33}}{3|\eta| + \frac{S_{0.33}}{S_{0.0}}(1-\xi^2)}$$

and:

$$\eta = p/q \quad ; \quad \xi = 27\det \boldsymbol{S}/2q^3$$

*(v)* Complementary conditions:

$$\dot{\gamma} \geq 0\,, \qquad \leq 0\,, \qquad \dot{\gamma} = 0.$$

## 3. NUMERICAL STRATEGY

In this section, it is presented the numerical strategy used to integrate the improved Lemaitre's model. The numerical model is based on an implicit academic finite element environment and the operator split methodology is further used to numerical integrate the improved constitutive formulation (see Simo *et al*., 1998), regarding an elastic predictor and a plastic corrector algorithms. The numerical integration algorithm for the improved model can be briefly presented in Box 2.

Box 2. Numerical integration algorithm for the improved Lemaitre's model with isotropic hardening and damage, and the denominator of damage function.

*(i)* Elastic trial state: Given the incremental strain $\Delta\varepsilon$ and the values of internal variables at pseudo-time $t_n$:

$$\boldsymbol{\varepsilon}_{n+1}^{e\,trial} = \boldsymbol{\varepsilon}_{n}^{e} + \Delta\boldsymbol{\varepsilon} \quad ; \quad R_{n+1}^{trial} = R_n \quad ; \quad D_{n+1}^{trial} = D_n$$

$$\tilde{\boldsymbol{S}}_{n+1}^{trial} = 2G\boldsymbol{\varepsilon}_{n+1}^{e\,trial} \quad ; \quad \tilde{p}_{n+1} = K\varepsilon_{v\,n+1}^{e\,trial} \quad ; \quad \tilde{q}_{n+1}^{trial} = \sqrt{\tfrac{3}{2}}\left\|\tilde{\boldsymbol{S}}_{n+1}^{trial}\right\|/(1-D_n)$$

*(ii)* Plastic admissibility:

If $\Phi^{trial} = \tilde{q}_{n+1}^{trial} - \sigma_y^{trial}\left(R_{n+1}^{trial}\right) \leq 0$, then

$(\cdot)_{n+1} = (\cdot)_{n+1}^{trial}$ ***(elastic step)*** go to *(v)*

*Else go to (iii)*

*(iii)* Return mapping algorithm ***(plastic step)***: Solve the system of equations below for $\Delta\gamma$, using *Newton-Raphson methodology*.

$$F(\ \gamma) \equiv \omega(\ \gamma) - \omega_n + \frac{\gamma}{\omega(\ \gamma)}\left(\frac{-Y(\ \gamma)}{S(\ \gamma)}\right)^{s} = 0$$

where,

$$\omega(\ \gamma) = \frac{3G.\ \gamma}{\tilde{q}_{n+1}^{trial} - \sigma_y(R_n + \ \gamma)}$$

$$-Y(\ \gamma) \equiv \frac{\left[\sigma_y(R_n + \ \gamma)\right]^2}{6G} + \frac{\tilde{p}_{n+1}{}^2}{2K}$$

$$S(\ \gamma) = \frac{S_{0.33}}{3\dfrac{\omega_{n+1}}{\left(\omega_{n+1} - \dfrac{3G\Delta\gamma}{\tilde{q}^{trial}}\right)}\left|\dfrac{\tilde{p}_{n+1}}{\tilde{q}_{n+1}^{trial}}\right| + \dfrac{S_{0.33}}{S_{0.0}}\left\{1 - \left[\dfrac{\left({}^{27}/_{2}\right)\det\tilde{\boldsymbol{S}}_{n+1}^{trial}}{\tilde{q}_{n+1}^{trial\,3}}\right]^2\right\}}$$

*(iv)* Update other state variables:

$$R_{n+1} = R_n + \ \gamma \quad ; \quad D_{n+1} = 1 - \omega(\ \gamma)$$

$$p_{n+1} = \omega(\ \gamma)\,\tilde{p}_{n+1} \quad ; \quad q_{n+1} = \omega(\ \gamma)\,\sigma_y(R_{n+1})$$

$$\boldsymbol{S}_{n+1} = \frac{q_{n+1}}{\tilde{q}_{n+1}^{trial}}\tilde{\boldsymbol{S}}_{n+1}^{trial} \quad ; \quad \boldsymbol{\sigma}_{n+1} = \boldsymbol{S}_{n+1} + p_{n+1}\boldsymbol{I}$$

$$\boldsymbol{\varepsilon}_{n+1}^{e} = \frac{1}{2G}\boldsymbol{S}_{n+1} + \frac{1}{3}\boldsymbol{\varepsilon}_{v\,n+1}^{e\,trial}\boldsymbol{I}$$

*(v)* Exit

## 4. NUMERICAL RESULTS

Regarding the numerical tests, an aluminum alloy 2024-T351 as selected, and a so-called "butterfly specimen" to represent loading condition within the range of low stress triaxiality ($0 \leq \eta < 0.33$). Furthermore, for high stress triaxiality ($\eta \geq 0.33$), cylindrical notched bars ($R = 4\ mm$ e $R = 12\ mm$) and a cylindrical smooth bar specimens were taken.

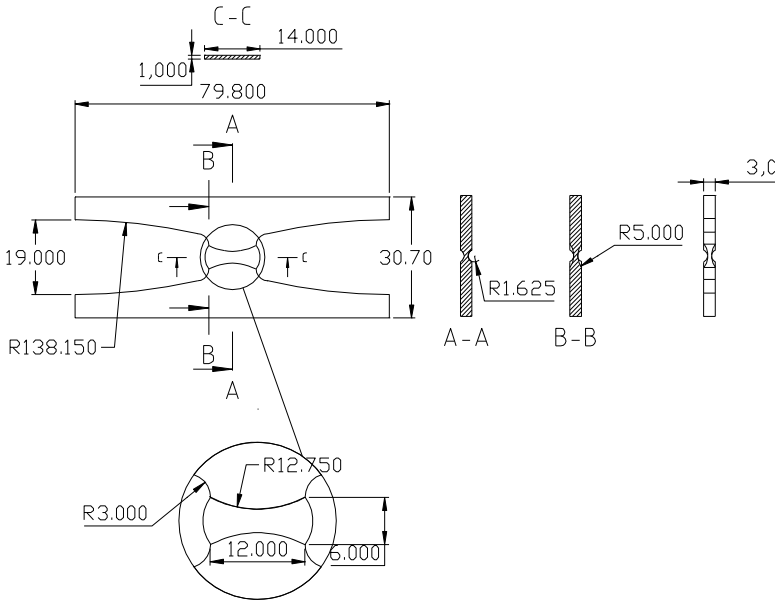


Figure 2. Geometry for the butterfly specimen (Bai, 2008).

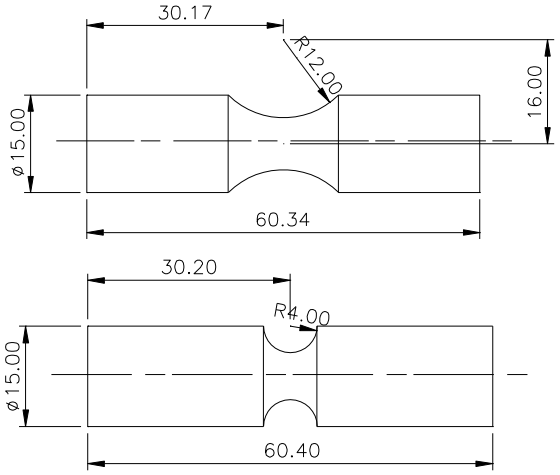


Figure 3. Geometries for an cylindrical notched bars (a) $R = 12.0\ mm$ and (b) $R = 4.0\ mm$ (Bai, 2008).

For the "butterfly specimen" a tridimensional finite element mesh is defined with 2432 elements of twenty nodes, followed by 12681 nodes, as presented in Figure 4. In this case, it is used a reduced integration strategy with nine Gauss points.

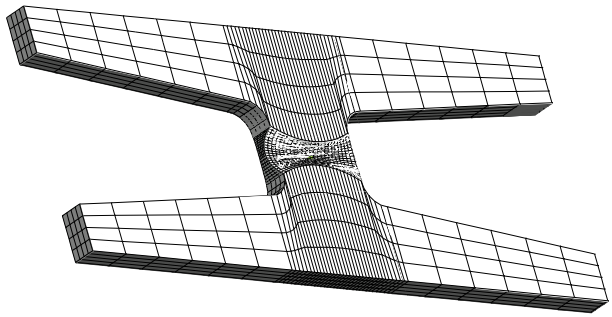

Figure 4. Tri-dimensional finite element mesh for the butterfly specimen.

For the cylindrical bars specimens, both of them were discretized with finite elements of eight nodes. A total of 1800 elements were used, followed by 5581 nodes. The lengths of gage used was $25.4\ mm$ for the aluminum alloy.. Due to the symmetry of the problems, only 1/4 of the specimens are simulated, regarding bi-dimensional problems.

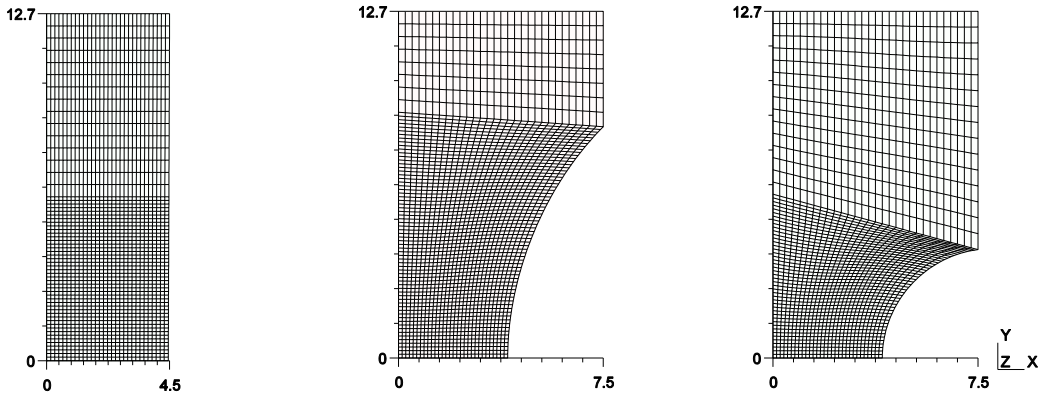


(a) (b) (c)

Figure 5. Finite elements meshes for cylindrical bars specimens, regarding Al 2024-T351.

Assuming the calibration procedure performed by Malcher et al (2013), the following material parameters are then determined as presented in Table 2.

Table 2. Material parameters for aluminum alloy 2024-T351.

| *Description* | *Symbol* | *Value* |
|---|---|---|
| *Modulus of elasticity* | $E$ | 72.400[$MPa$] |
| *Poisson's ratio* | $\nu$ | 0.33 |
| *Initial yield stress* | $\sigma_{y_0}$ | 352.00 [$MPa$] |
| *Hardening curve* | $\sigma_y(R)$ | $908.(0.0058 + R)^{0.1742}$ |
| *Critical damage* | $D_c$ | 0.26 |
| *Exponent of damage* | $s$ | 1 |
| *Denominator of damage (high triaxiality)* | $S_{0.33}$ | 6 [$MPa$] |
| *Denominator of damage (low triaxiality)* | $S_{0.00}$ | 8.25 [$MPa$] |

As a first analysis, are presented by Figure 6, the reaction curves determined numerically using the new formulation, and the original model, and experimentally, taken hand the butterfly specimen, subject to pure shear (Figure 6a), the cylindrical smooth bar specimen (Figure 6b) and cylindrical notched bars specimens $R = 12\ mm$ (Figure 6c) and $R = 4\ mm$ (Figure 6d), both subjected to pure tension. It can be observed with the introduction of the denominator of damage function, that the displacement at fracture, determined numerically by the new formulation, is now closer to the experimentally observed, considering all the specimens evaluated here. Regarding the original Lemaitre's model, for loading conditions resulting in high level of stress triaxiality ($\eta \geq 0.33$), the model predicts the fracture onset so late (cylindrical notched bars specimens). Furthermore, for loading conditions within the range of low stress triaxiality, as pure shear ($\eta = 0$), the model predicts the fracture onset prematurely. However, with the new formulation, the predictive ability becomes more uniform, so that the model is now less sensitive to relation between the conditions of use versus the calibration condition.

Table 3 presents the displacement values for experimental tests and numerical simulations. It appears that the difference between the numerical and experimental displacement, considering the original Lemaitre model is approximately 17%, 27% and 68%, respectively, for the butterfly specimen (pure shear), notched bar $R = 12\ mm$ (pure tensile) and notched bar $R = 4\ mm$ (pure tensile). With the new formulation and reduced dependence on the calibration condition, in both cases the difference between numerical results and the experimentally observed values is reduced to approximately 1%.

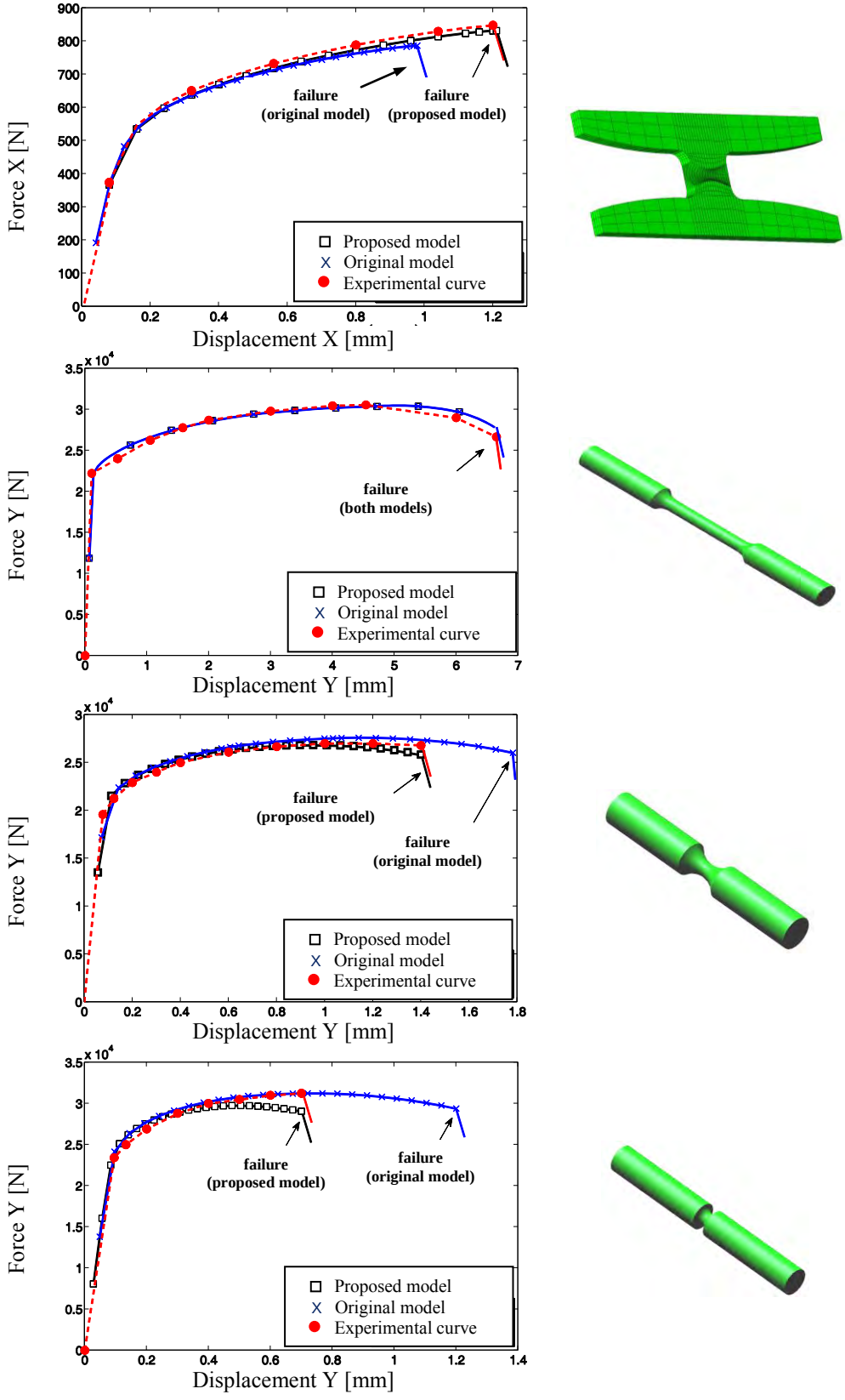


Figure 6. Reaction curves for aluminum alloy 2024-T351.

Table 3. Assessment between experimental and numerical displacement at fracture (aluminum 2025-T351)

| Specimen | $\eta$ | Displacement at fracture (mm) | | |
|---|---|---|---|---|
| | | | Model | |
| | | Experimental data | original | Improved |
| Butterfly | 0.00 | 1.18 | 0.97 | 1.20 |
| Smooth bar | 0.33 | 6.65 | 6.65 | 6.65 |
| Notched bar $R = 12\ mm$ | 0.47 | 1.40 | 1.78 | 1.41 |
| Notched bar $R = 4\ mm$ | 0.74 | 0.70 | 1.18 | 0.71 |

## 5. CONCLUSIONS

Thus, the improved Lemaitre's model can then be calibrated taken hand two points and used to determine the correct displacement at fracture regarding wide range of stress triaxiality. The improved model demonstrated the same high performance, both in regions of low and in high level of stress triaxialities, independent of the material used for analyze.

## REFERENCES


Bai, Y. (2008). Effect of Loading History on Necking and Fracture. Ph.D Thesis, Massachusetts Institute of Technology.

Bai, Y., Wierzbicki, T. (2008). A new model of metal plasticity and fracture with pressure and Lode dependence, International Journal of Plasticity, 24:1071-1096.

Brünig, M., Chyra, O., Albrecht, D., Driemeier, L., Alves, M. (2008). A ductile damage criterion at various stress triaxialities, *International Journal of Plasticity*, 24: 1731–1755.

Chaboche, J.L. (1984). Anisotropic Creep Damage in the Framework of Continuum Damage Mechanics. Nuclear Engineering and Design,79: 309–319.

Gao, X., Zhang, T., Zhou, J., Graham, S.M., Hayden, M., Roe, C. (2011), On stress-state dependent plasticity modeling: Significance of the hydrostatic stress, the third invariant of stress deviator and the non-associated flow rule, International Journal of Plasticity, vol. 27, 2:217-231.

Johnson, G.R, Cook, W.H. (1985). Fracture characteristics of three metals subjected to various strains, strain rates, temperatures and pressures. Engineering Fracture Mechanics, 21(1):31–48.

Krajčinović, D., Fonseka, G.U. (1981). The Continuous Damage Theory of Brittle Materials – Part 1: General Theory. J. Appl. Mech., 48, 809–815.

Lemaitre, J. (1985). A continuous damage mechanics model for ductile fracture. Journal of Engineering Materials and Technology - Trans. of the ASME, 107:83–89.

Malcher, L. ; Andrade Pires, F.M. ; César de Sá, J.M.A., (2013), An Extended GTN Model for Ductile Fracture under High and Low Stress Triaxiality. International Journal of Plasticity (submitted).

Murakami, S. and N. Ohno (1981). A continuum theory of creep and creep damage. Proceedings of 3rd IUTAM Symposium on Creep in Structures. A. R. S. Ponter and D. R. Hayhurst. Leicester, England, Springer-Verlag: 422–444.

Nahshon, K., Hutchinson, J. (2008). Modification of the Gurson model for shear failure. European Journal of Mechanics A/Solids, 27:1–17.

Simo, J.C., & Hughes, T.J.R. (1998). Computational Inelasticity. New York: Springer-Verlag.

Tvergaard, V. (2008). Shear deformation of voids with contact modeled by internal pressure. *International Journal of Mechanical Sciences*, 50:1459–1465.

Zadpoor, A.A., Sinke, J., Benedictus, R. (2009). Formability prediction of high strength aluminum sheets, *International Journal of Plasticity,* 25:2269–2297.